

# Optimization of Material Properties and Process Parameters for Tube Hydroforming of Aluminum Extrusions

Adam R. Loukus

Ghatu Subhash<sup>1</sup>

e-mail: subhash@mtu.edu

Mehdi Imaninejad

Department of Mechanical Engineering-  
Engineering Mechanics,  
Michigan Technological University,  
Houghton, MI 49931

*Analysis of process optimization for hydroforming of central-bulge and T-branch from AA6063 tubes is conducted for W-temper and T4 heat-treated conditions. Systematic characterization of AA6063 mechanical properties as a function of aging time was also conducted. It was found that hydroforming in the W temper facilitates forming of a bigger T branch (due to available greater ductility), but limits the strength (hardness) of the final component compared to that formed in the T4 condition. By optimizing the material heat-treatment conditions and the process parameters during hydroforming, strains well in excess of the traditional forming limits can be achieved in the finished components. The relevant microstructural kinetics during hydroforming of the above two geometries in the two heat treated conditions and the associated strengthening mechanisms in aluminum alloys are discussed. [DOI: 10.1115/1.2400259]*

## 1 Introduction

Recent success of aluminum tube-hydroformed components in the automotive industry has been a driving force for numerous additional investigations into suitable alloy composition, influence of process parameters on forming limit diagram (FLD), and optimization of hydroforming process parameters, such as the correlation between axial feed and internal pressure, etc. [1–10]. Tube hydroforming using aluminum alloys has been of interest to the industry because components made of aluminum offer several benefits such as weight savings and superior corrosion resistance compared to steels. It is well known that at room temperature, aluminum exhibits lower ductility than steel and hence there is a smaller forming process window to successfully produce a complex part or to avoid incipient failures such as bursting, wrinkling, and buckling [4,11]. Other considerations include loss of strength and stiffness when aluminum is substituted for steels. Some of these shortfalls are alleviated either by the addition of stiffeners to a structure or by precipitation heat treatment of the final component (i.e., artificial aging) which strengthens the material. In light of these challenges confronting the use of aluminum hydroformed components, optimization of the process parameters to enhance process times, and component integrity is increasingly essential as the demand for these components continues to grow in the automotive industry. In a recent work by Johnson et al. [12] an optimization scheme for 6061-T4 aluminum was developed using tensile data and plasticity theory to control the material feed in the hydroforming process. The current research uses tensile test data in an optimization scheme to maximize the bulge height without excess thinning in the hydroformed section.

Aluminum 6xxx series alloys are attractive to the industry for components requiring medium strength because of their ability to be heat treated. The commercial aluminum alloy 6063 (AA6063) was utilized in this study to determine the feasibility of its use in

hydroformed components. The alloy was hydroformed in two conditions: solution treated and quenched, called “W temper,” and in the naturally aged condition called “T4.” There are benefits from hydroforming in both of these conditions. Aluminum in the T4 condition has moderate ductility and good strength, and therefore requires no further heat treatment after forming. However, due to its higher strength in this condition, the alloy is more difficult to form or it requires higher press capacity. On the other hand, aluminum alloys in the W temper exhibit better formability than alloys in the aged condition (i.e., T4 and T6 conditions) and therefore it is easier to conduct forming operations [13] or produce complex geometries. However, it is not known how these two conditions influence the final strength of the hydroformed section. To quantify the influence of the above two heat-treatment conditions on the final part, two geometries were chosen in this investigation: a hydroformed central bulge using a closed die and a T branch (Figs. 1 and 2). In the closed-die configuration, the process was optimized for tube conformance to the die geometry and minimal thickness variation in the hydroformed region. The material strength (hardness) over a time period was then monitored. For the T-branch configuration, the process was optimized to achieve the highest possible bulge height and minimal thickness variation. The measured thickness values in the T branch were then compared to the numerical simulations for model validation.

## 2 Analysis Procedure

Round tubular AA6063 extrusions (38.1 mm outer diameter  $\times$  3.18 mm thick) were obtained from Hydro Aluminum Technology Center, NA in Holland, Mi. Uniaxial tensile, Vickers (macro) hardness, and hydroforming experiments were performed on this material to determine the material properties and to investigate the material behavior in the above two heat-treated conditions. The following steps illustrate the approach.

1. Tensile bars were cut (as per ASTM-B557M) from the tubes in the longitudinal direction and heat treated to W temper and T4 conditions. Uniaxial tensile tests were conducted on these specimens at a rate of 5 mm/min in a servo-hydraulic test machine. The resulting tensile curves were fit with the power-law model,  $\sigma = Ke^n$ , to extract the  $K$  and  $n$  values for

<sup>1</sup>Corresponding author. New address: Mechanical and Aerospace Engineering, University of Florida, Gainesville, FL 32611. email: subhash@ufl.edu

Contributed by the Materials Division of ASME for publication in the JOURNAL OF ENGINEERING MATERIALS AND TECHNOLOGY. Manuscript received March 10, 2005; final manuscript received July 31, 2006. Review conducted by Mark F. Horstemeyer.

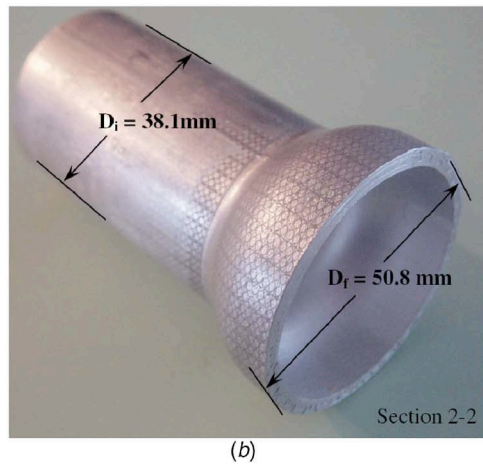
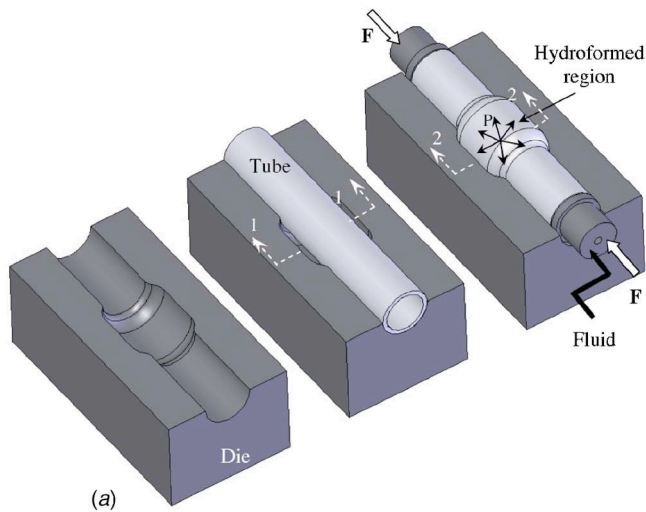


**Fig. 1 (a) Schematic of the closed-die geometry to produce a central bulge using hydroforming; and (b) a portion of hydroformed tube revealing the final dimensions**

each heat-treated condition. This material model was later used in LS-DYNA simulations of the tube hydroforming process to produce a central bulge using a closed die as shown in Fig. 1. Using LS-OPT, in conjunction with LS-DYNA, the optimum loading paths for internal pressure and axial feed were determined to achieve tube conformance to the die geometry. The optimization method will be discussed in the next section.

2. Once the optimized feed paths were determined by simulations for the two heat-treated conditions, experiments were conducted in a hydroforming press to verify if these simulated feed paths produced a successful part shown in Fig. 1. Surface strains on the hydroformed section were measured to verify that the tubes experienced equivalent strains for both heat-treated conditions. The Vickers hardness was then measured on the cross section of the central portion of the formed region, shown schematically in Fig. 1(b). The goal was to form the tubes to the same strains in different heat-treatment conditions and then observe differences in the hardness over aging time. Comparisons were made between the tubes that were hydroformed in the W temper followed by aging and the tubes that were first naturally aged for a period of time (T4) and then hydroformed.
3. Using an approach similar to step (1), a T branch was simulated, see (Fig. 2). Note that large strains (well in excess of those achieved in the closed-die experiments) are now re-

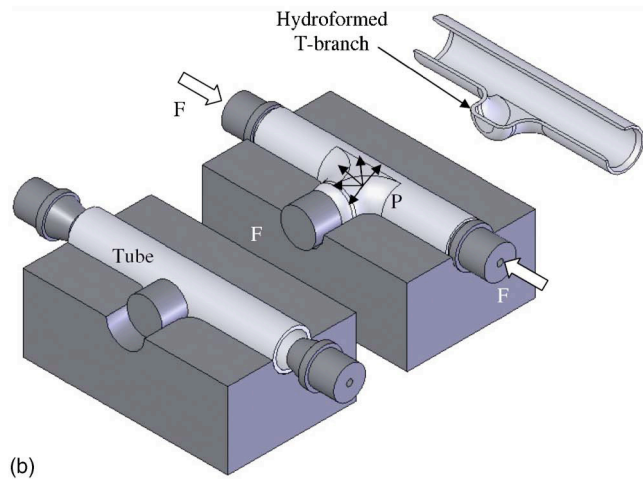
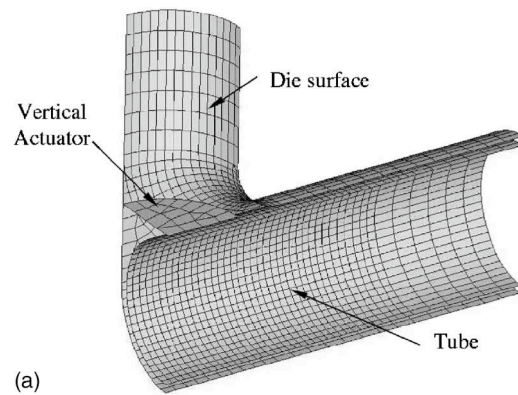


**Fig. 2 (a) FE meshed geometry and (b) schematic of the setup for hydroforming of T-branch**

quired to form a T branch. Because our intent was to achieve the maximum possible height of a T branch, the differences in the plastic behavior under the above two heat-treated conditions will play a major role in the formation of the final product and its properties. It is believed that increased ductility (i.e., higher T branch) can be derived from the material if it is formed in the W temper. However, for completeness, both conditions were optimized for T-branch formation and then experiments were performed in a specially designed die to verify the simulated results.

4. Upon completion of the T-branch experiments, the surface strains were measured by strain measuring software, CamSysGPA v1.0, to create a map of strains experienced by the material at various locations of the T branch. The thicknesses at various locations on the central cross section of the experimental T branch were measured and compared to the numerical results.

### 3 Optimization Method

Recall that in closed-die hydroforming two process variables, axial feed and internal pressure, are involved. However, the sequence of loading paths and the amplitude of loading need to be determined to obtain full conformance of the tube to the die geometry. One could imagine that there are an infinite number of paths available to achieve the given objective. Depending on the constraints chosen, the derived optimum path could be different. For a T branch, the situation is even more complex because of the additional variable, the vertical feed, required to avoid premature bursting of the tube by applying backpressure in the expanding zone. Clearly, the sequence, the path, and the amplitude of these three process parameters must be optimized to obtain the maxi-

imum T-branch height. The optimization procedure for both of the above geometries is briefly described in the following.

The optimization problem can be defined mathematically as [3]

$$\begin{cases} \text{optimize } f(p), p \in D \\ \text{subject to } g_i(p) \leq 0, & i = 1, 2, \dots, m \end{cases} \quad (1)$$

where  $f(p)$  is the “objective” or “cost” function that needs to be optimized, e.g., maximum bulge height (T branch) or minimum volume difference between tube and die (closed die);  $p$  is the design variable, such as end feed or vertical feed or internal pressure; and  $D$  is the feasible domain from which the design variables can be chosen. The  $g_i(p)$  are the “constraint” functions such as effective stress or strain or minimum thickness experienced by the tube during the hydroforming process.

From the above discussion, it can be envisioned that the optimum feed paths for each of these hydroforming operations, closed die or T branch, could be highly nonlinear. It is possible, in the optimization program (LS-OPT), to obtain nonlinear feed paths for the actuators and the internal pressure, but the process is computationally expensive. It is therefore beneficial to approximate the paths with linear segments. Imaninejad et al. [9] and Al-Qureshi and Filho [14] have concluded that increasing the number of load path segments approximating the optimum load curve not only increases the computational efficiency but also produces final components with uniform thickness distribution and/or larger bulge heights. It was also shown [9] that a two-segment (stroke) path produces results comparable to a quadruple-stroke path. This result was expected because the tube was allowed to yield mostly by the application of internal pressure and with minimal axial feed during the first part of the loading stroke. During the second stroke, the axial feed was increased linearly to feed material into the expanding zone. Accordingly, a two-stroke path was chosen for the axial feed in the current study. In the experimental facility available at Michigan Technological University (MTU), shown in Fig. 3(a), the control software only allows a single pressurizing rate for the internal pressure path. Typical process paths for these variables are shown graphically in Fig. 3(b). Thus, the variables to be optimized are: the axial feed end values  $AF_1$  and  $AF_2$ , the final pressure ( $P$ ) (these three are common for both closed die and for T branch), and the vertical feed values  $BH_1$  and  $BH_2$  (T branch only). Thus, there are five values to be estimated and optimized in the latter geometry.

For closed-die forming shown in Fig. 1, the objectives of the optimization problem were to minimize the volume between the die and the tube, and also to maintain a uniform thickness distribution in the hydroformed section. To avoid failure, a constraint was imposed where the effective stress in each element  $\bar{\sigma}_i$  is less than the ultimate tensile strength  $\sigma_u$  of the material. Thus, the objectives and the constraints for closed-die formation can be written as

*Objective (1): Minimize* (Volume<sub>Die</sub> - Volume<sub>Tube</sub>)

*Objective (2): Minimize* thickness deviation  $f(p)$  where

$$f(p) = \sqrt{\sum_{i=1}^N \left( \frac{t_i - t_o}{t_o} \right)^2} \quad (2)$$

*Constraint (1):*  $\bar{\sigma}_i < \sigma_u$

where  $t_i$  is the current elemental thickness and  $t_o$  is the original tube thickness. To obtain the thickness values at various locations of the tube during hydroforming, the LS-OPT program scans through the results of LS-DYNA while ensuring that the constraints are not violated and the objectives are met as it attempts to find suitable axial feed ( $AF_1$  and  $AF_2$ ) and internal pressure ( $P$ ) values.

Figure 2(a) shows the finite element (FE) mesh of the T branch modeled using quadratic shell elements in HyperMesh v5 and exported to LS-DYNA. The die geometry was modeled using rigid shell elements. Due to the symmetry, only 1/4 of the die was

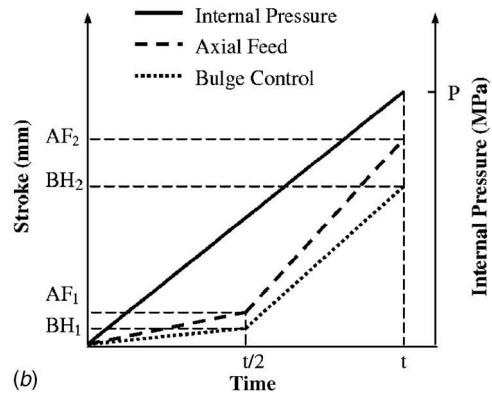
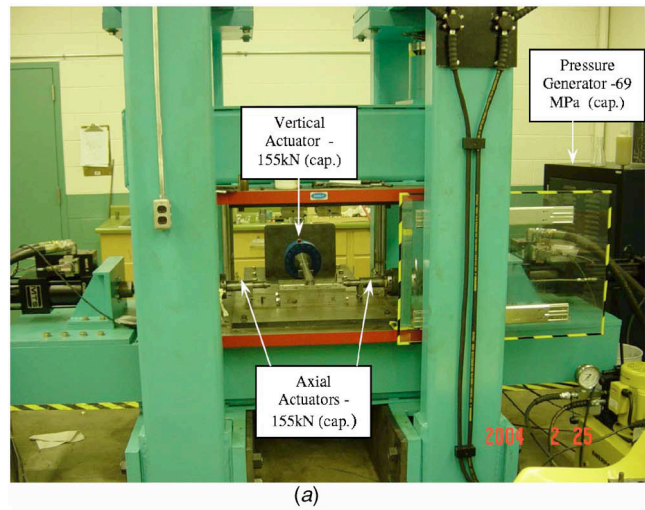


**Fig. 3 (a) Hydroforming press (3500 kN closing capacity) at MTU and (b) schematic of the typical optimized feed path**

modeled and symmetric boundary conditions were applied along the boundary planes. In the T-branch simulations, shown in Fig. 2(b), the primary objective was to obtain a large bulge height without failure. Therefore, the objective was changed to

*Objective (1): Maximize* branch height (or vertical feed)

$$\text{Constraint (1): } t_{\min} < t < t_{\max} \quad (3)$$

where  $t_{\min}$  and  $t_{\max}$  are the minimum and maximum allowable thicknesses, respectively. The rationale for choosing the appropriate  $t_{\min}$  and  $t_{\max}$  values will be described later. Notice that the constraint is now based on thickness (strain) in each element instead of stress. The rationale to constrain the tube thickness is based on contact considerations. Due to severe stresses at the tube–die interface in the nonexpanding regions, the effective stress experienced in these noncritical areas may exceed the material ultimate stress well before failure is experienced in any of the critical expanding regions. Thus, if a stress constraint (such as  $\bar{\sigma}_i < \sigma_u$ ) is imposed, the achievable T-branch height may be limited. Upon each iteration through LS-DYNA, a set of values is chosen by LS-OPT for the three process variables (axial feed, vertical feed, and internal pressure). It then scans through all the elemental results from the FE model and searches for any violation of the imposed constraints. If there is a violation, LS-OPT chooses another set of values to avoid another violation of the constraint. This procedure usually results in decreasing the value of the process variables to avoid repeated violation of the set constraints, and consequently gives rise to a shorter T branch. To achieve the maximum bulge height (BH) of the T branch, the set constraints must keep the tube from failing, but allow for the successful formation of a large T branch. This can be effectively

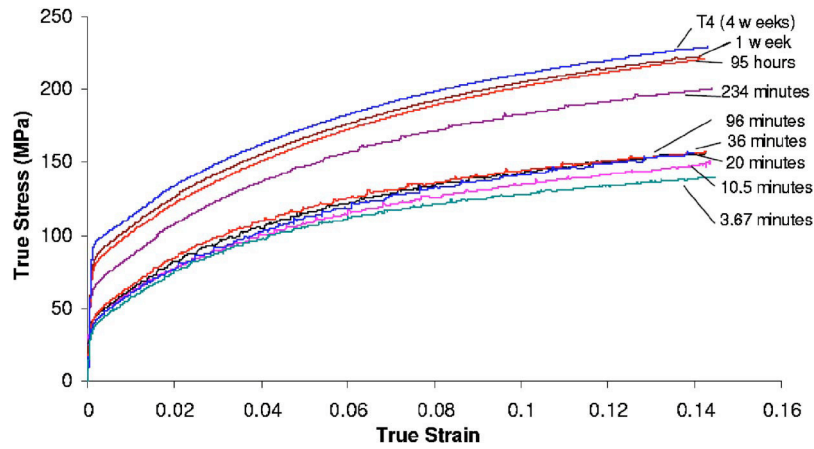


Fig. 4 Tensile response of AA6063 as a function of aging time after solution treatment and quenching operation

achieved by using thickness as the constraint. In this analysis,  $t_{\min}$  was set equivalent to a thickness strain of half of the hardening coefficient, i.e.,  $n/2$ . This value of  $t_{\min}$  was chosen because it has been shown in tube hydroforming (THF) that instability occurs when the thickness strain reaches a value of  $n/2$  when the ends of the tube are constrained [13,15]. The maximum thickness of the tube,  $t_{\max}$ , was arbitrarily chosen (to avoid excess thickening of the tube walls in some regions) corresponding to a thickness strain equal to the value of  $n$ . For all the simulations a predetermined Coulomb friction coefficient of 0.05 is used between the tube and die cavity. The friction coefficient was determined by a forced-end THF experiment where the difference in the forces at the two ends is used as the friction force. Knowing the tube area in contact and the internal pressure (that causes the normal force), the friction coefficient was calculated. For more details the reader is referred to Imaninejad et al. [7].

#### 4 Effect of Heat Treatment

**4.1 Tensile Test Results.** To determine the mechanical properties of heat-treated AA6063, the tensile specimens were solution treated at a temperature of 510°C for 10–15 min and then water quenched resulting in W-temper condition. Tensile tests were con-

ducted at regular time intervals starting immediately after quenching (W temper) until the material naturally aged for several hundred hours (T4 condition). The true stress–true strain curves are shown in Fig. 4.

There are several important features to note from the stress–strain responses. The curves clearly show the effect of natural aging time on the material behavior, i.e., the longer the interval between quenching and the tensile tests, the higher the yield strength and the flow stress. The significant change in material behavior within the first few hours of natural aging indicates that W temper is unstable and with passage of time, the material ages to the more stable T4 condition. This behavior is reflected as the frequent occurrence of serrations in the stress–strain curves (called the Portevin–LeChatelier (PLC) effect) of the samples tested immediately after quenching [16]. The frequency of these serrations reduces dramatically with aging. After approximately 4 days of natural aging, the curves tend to become smooth reflecting the T4 condition. The kinetics of this process is discussed later in Sec. 6.

Each of the curves in Fig. 4 was fit using the power-law model ( $\bar{\sigma} = K\bar{\epsilon}^n$ ) to extract the strength coefficient,  $K$ , and the hardening coefficient,  $n$ , values. The value of  $n$  was calculated from the slope of the stress strain curve plotted on a log–log scale. The data are fitted from the yield point up through the ultimate tensile strength for all of the tested materials. The curve fit for the data was well within an  $R^2$  value of greater than 0.99. The yield stress and the  $n$  values are plotted in Fig. 5. Note that the yield strength increases and the hardening coefficient decreases as the material ages at room temperature, indicating a loss of ductility in the material. The aging occurs rapidly in the hours immediately following the quenching operation and stabilizes after around 100 h. Table 1 shows the relevant  $K$  and  $n$  values from the material in the W temper (average of tests through 96 min) and T4 conditions (average of tests >5 days).

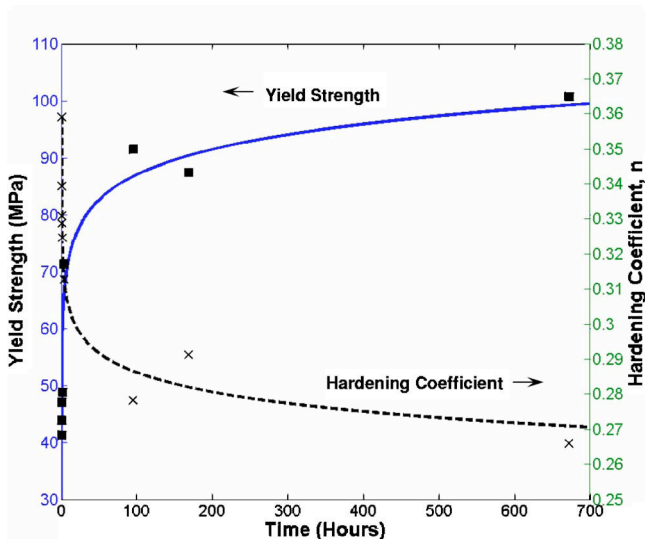


Fig. 5 Variation of yield strength and hardening coefficient as a function of aging time

**4.2 Closed-Die Hydroforming.** Employing the material properties derived from the previous section, the closed-die (Fig. 1(a)) central bulge simulations were conducted. The optimized values for axial feed and internal pressure are shown in Table 2. It is seen that the simulated end-feed results for both W temper and

Table 1 Tensile data for input into FE model

	W temper	T4
Strength coefficient, $K$ (MPa)	308	386
Hardening coefficient, $n$	0.340	0.266

**Table 2 Optimized axial feed and internal pressure values for closed-die hydroforming**

	W temper	T4
AF <sub>1</sub> (mm)	5.12	5.06
AF <sub>2</sub> (mm)	13.34	13.47
P (MPa)	41.37	63.16

T4 condition are almost the same. This result is because the material is not stretched to its limit but confined to a given geometry (closed-die, see Fig. 1(a)) allowing limited expansion primarily due to internal pressure. As expected, the internal pressure is significantly larger for the T4 material due to its higher strength. Using the above optimized values, the closed-die hydroforming experiments were performed on the aluminum tubes. A circular grid of 1.27 mm (0.50 in.) diameter was etched onto the surface of the undeformed tube to monitor the surface strains after hydroforming in both heat-treatment conditions. A typical original tube and the hydroformed tube are shown in Fig. 6. The hydroformed tubes were cut at the midsections (see Fig. 1(b)) and the hoop strain and the thickness were measured to verify that they were hydroformed to the same strain. The final hoop strain (measured from the etched grid) and thickness strain in both tubes were 0.28 and -0.09, respectively. To monitor the strength of the hydroformed region of the tube as a function of aging time, tubes were hydroformed in the W-temper condition (i.e., 10 min after quenching) and in the T4 condition (aged for 5 days). The Vickers hardness (at 10 kg load) was measured before and after hydroforming. The results are shown in Fig. 7. In this figure, the data with label “W\_HF\_AGE” refers to being hydroformed in W-temper condition and then aged, and “W-AGE-HF” refers to being aged from W temper to T4 condition and then hydroformed. For completeness, the Vickers hardness data on an undeformed tube W tempered and then aged to 170 h is also shown (indicated as “W-AGE”). In all of the above tests, eight hardness measure-

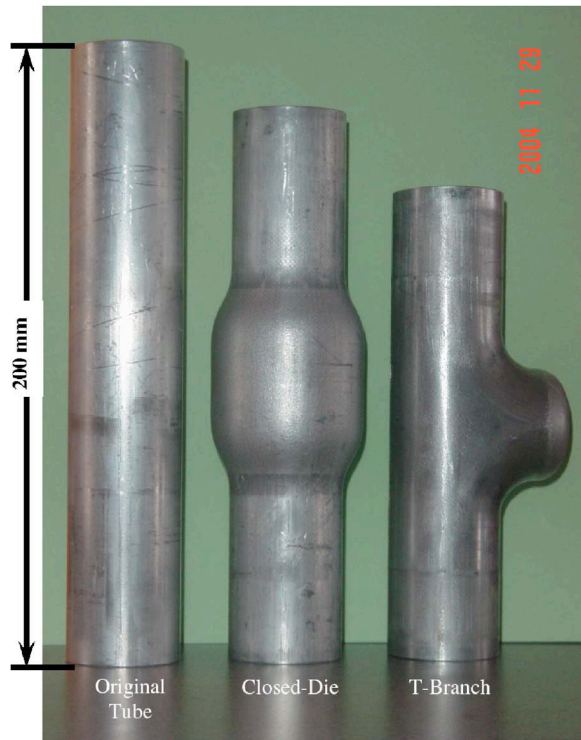


**Fig. 6 Original and hydroformed aluminum tubes**

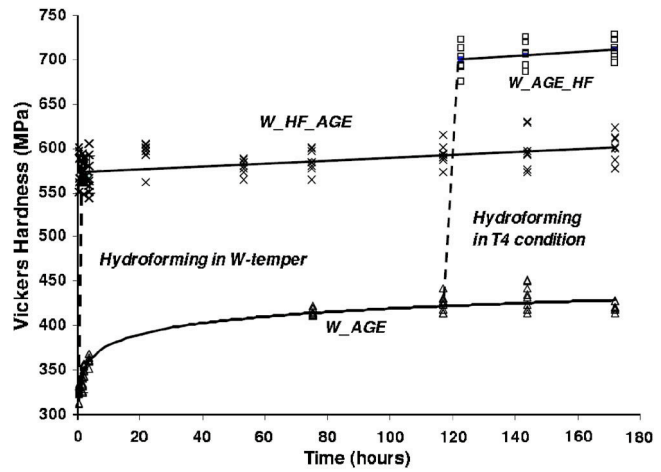


**Fig. 7 Vickers hardness (at 10 kg load) as a function of natural aging time before and after closed-die hydroforming**

ments were conducted at each time interval. Because the average grain size in the AA6063 alloy was around 100–150  $\mu\text{m}$ , a 10 kg load was used for Vickers hardness measurements so that the imprint covered a statistically significant number of grains.

The following observations can be made from the plot: (1) The hardness versus aging time (W-AGE) for AA6063 shows a response similar to that seen for the yield stress in Fig. 5, i.e., hardness increases rapidly with the natural-aging time initially and then stabilizes after reaching the T4 condition. (2) Hydroforming (or any plastic deformation) in both W temper or T4 conditions increases the hardness of the component significantly, as indicated by the dashed line. This behavior is typical of materials that exhibit hardening response during plastic deformation [17]. (3) After hydroforming, however, the material shows little or no response to further aging, i.e., the material does not strengthen with time after plastic work. (4) Forming in the W temper influences the aging response of the material, i.e., the material is stabilized immediately upon hydroforming or plastic work. (5) The material which is allowed to age for 5 days (120 h) follows the aging response as expected and reaches the T4 condition. Note that upon hydroforming there is a significant increase in hardness. The resulting final hardness of the two hydroformed tubes (although formed to the same strain) are not equal even after the same amount of aging is allowed, i.e., the material which has been aged first to the T4 condition and then hydroformed has a higher Vickers hardness than the material hydroformed in W-temper condition and then aged. The significant difference in final hardness values of the two hydroformed tubes shows that forming immediately after quenching has a detrimental effect on the final component strength and its ability to age naturally. The associated mechanisms are further discussed in Sec. 6.

Although the W-temper condition results in lower hardness, there are some advantages to forming a material in this condition as evident from the data acquired from the tensile responses (Figs. 4 and 5). The inherently lower yield strength and higher  $n$  value in the W-temper alloy provide higher ductility and allow the material to form into more complex shapes than is possible with the material in the T4 condition, i.e., W temper provides a larger process window. For example, the use of material in the W temper to form a T-branch may result in realizing the full potential of forming AA6063 to obtain the maximum T-branch height. However, the final strength of the component is compromised when compared to the tubes formed in the T4 condition.

## 5 T-Branch Hydroforming

Similar to the previous closed-die hydroforming, the optimal process paths for horizontal and vertical actuators, and for the

**Table 3 Optimized process parameters and the resulting bulge heights for the T branch**

Parameter	Symbol	W temper	T4
Pressure (MPa)	$P$	41.27	63.16
Axial feed (mm)	$AF_1$	1.14	4.814
	$AF_2$	29.91	24.12
Vertical feed (mm)	$BH_1$	9.436	5.009
	$BH_2$	24.68	19.89
Final bulge height (FE)	$BH_{FE}$	24.18	19.39
Final bulge height (exp)	$BH_{exp}$	23.00	20.22
Max. effect stress	$\sigma_{eff}$	275.3	364.1

internal pressure, were obtained for the T branch under the set constraints and objectives. The resulting simulated end values are given in Table 3. It is shown that during the first part of the simulation, the axial feed  $AF_1$  and the vertical feed (i.e., bulge height,  $BH_1$ ) values are small. This indicates that any deformation of the tube is due strictly to the internal pressure. The axial feed is just enough to seal the ends and avoid leaking of the incompressible fluid (water). The program allows the internal pressure to build up which causes the material to yield before the end actuators initiate substantial feeding of the material into the expanding

zones. Accordingly, the end-feed ( $AF_2$ ) and the bulge height ( $BH_2$ ) increase dramatically during the second stroke. These bulge heights are predicted by the simulation without violating the constraint,  $t_{min} < t < t_{max}$ .

Using the above optimized paths, experiments were conducted on tubes to form a T branch in both the heat-treated conditions. A circular grid was etched onto the surface of the undeformed tube (see Fig. 8) to monitor the surface strains. The experimental bulge heights measured from the tubes were 23.00 mm and 20.22 mm for the W-temper and T4 conditions, respectively. These values are within 5% of the simulated values of 24.18 mm and 19.39 mm, respectively, for both material conditions. The observed deviations from the simulated results are mainly due to some limited features of the hydroforming press. For example, the vertical actuator does not have enough precision to move the exact displacement prescribed by the controller, and hence the final bulge height may have been affected. The computed stresses from the FE model, shown in Table 3, indicate that the effective stress exceeds the ultimate tensile stress (UTS) measured in the tensile tests of the material. The measured maximum UTS values for 6063-W and 6063-T4 are 180 MPa (96 min) and 230 MPa (T4), respectively. Clearly, the effective stress may not be a suitable constraint to use in hydroforming if the contact stresses are large and when a large T branch is desired. The resulting parts did not

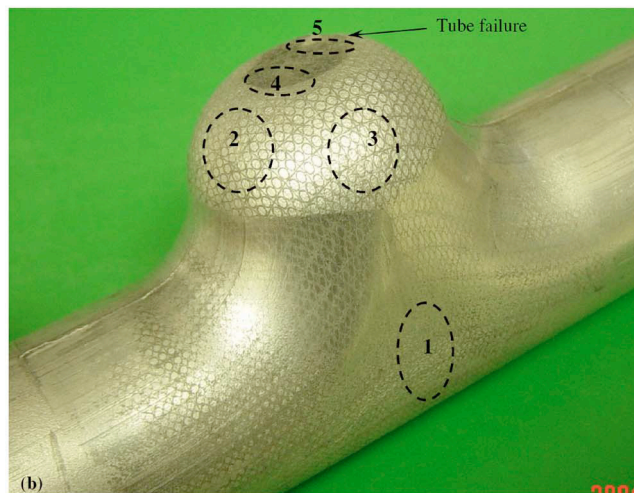
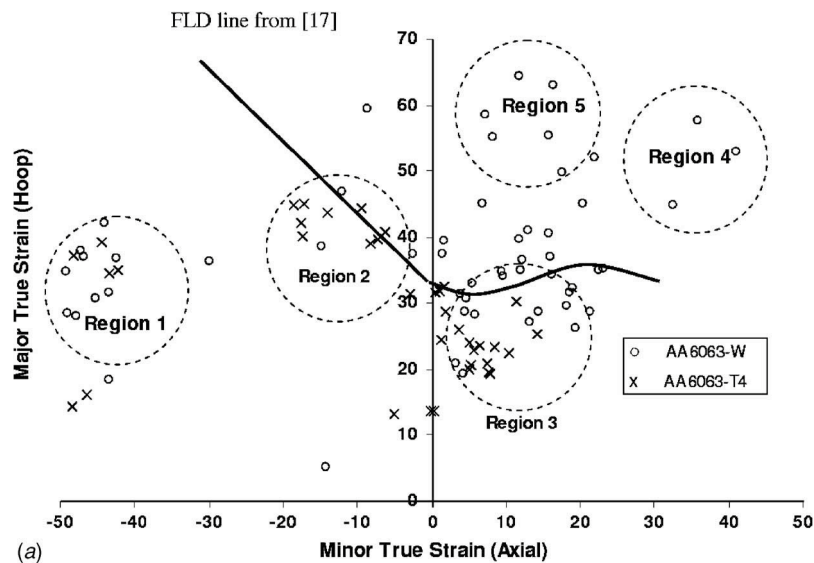


**Fig. 8 (a) Surface strains plotted on a FLD measured from regions indicated on the hydroformed tube shown in (b)**

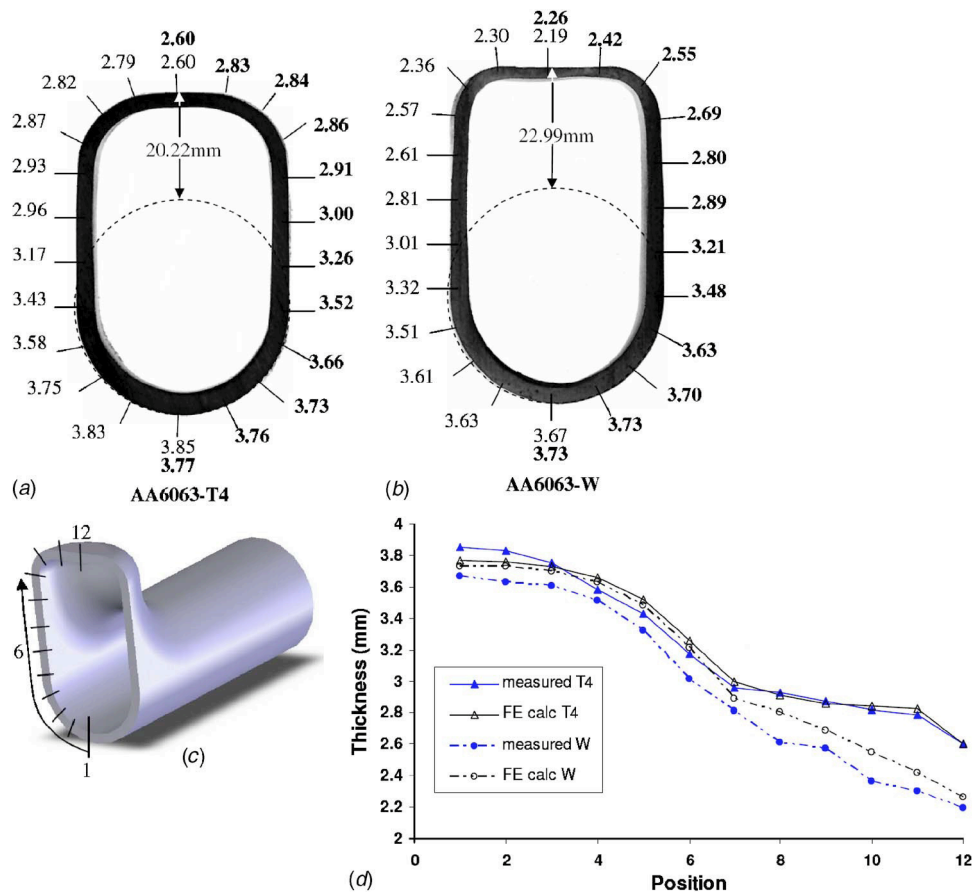


**Fig. 9 Comparisons of thickness between experiments and FE simulations (in bold) of T-branch on (a) and T4 and (b) W-tempered materials. The dotted lines indicate the outer diameter of the undeformed tube. (c) Location of thickness measurements on the T-branch. (d) Plot of thickness values versus position.**

fail (see Fig. 6) and did not violate the thickness constraints. Therefore, it is further confirmed that the set thickness limits are better constraints (than stress) to be used in the optimization method for tube hydroforming.

The surface strains measured from the deformed grid on the T branch of AA6063-W and AA6063-T4 are plotted on a FLD shown in Fig. 8(a). The regions from which the above data were extracted on the workpiece are indicated in Fig. 8(b). Also indicated in the figure is the forming limit line from Marciniak and Duncan [18] for an  $n$  value of 0.34 (AA6063-W). The plot indicates that significantly higher hoop strains ( $\epsilon_h$ ) beyond the forming limit line can be achieved with the optimized process paths without causing tube failure. These strains typically occur on the top of the T branch. Also shown in Fig. 8(a) are the strains measured from a tube (AA6063-W) which was allowed to fail. These strains near the failure zone are shown in Region 5. It has been shown in the literature [10,11] that instability occurs in the tube hydroforming process when the thickness strain reaches a value of  $-n$  in a tube where the ends are not constrained. From volume constancy, the thickness strain is  $\epsilon_t = -(\epsilon_h + \epsilon_a)$  where  $\epsilon_h$  and  $\epsilon_a$  are the hoop and axial strains, respectively. It can be calculated from the strains plotted in Fig. 8(a) and the above equation, that the thickness strain exceeds the value of  $-n$  in some locations (e.g., Region 4) of the optimized parts. As expected, in the regions away from the T branch, the thickness of the tube increases (e.g., Region 1) due to the material in-flow due to the axial feed (of nearly 25 mm from each end) (see Table 3 and Fig. 6). Regions 2 and 3 experience significantly large hoop strains, with moderate nega-

tive and positive axial strains, respectively. From volume constancy, it can be seen that both regions experience severe thinning.

To validate the FE simulations, the experimentally measured thickness along the cross section of the T branch was compared to the simulated thickness values. Figs. 9(a) and 9(b) show the thickness measurements taken from the base to the top of the T branch as indicated in Fig. 9(c). On the left side of Figs. 9(a) and 9(b), the experimentally measured thickness values are indicated for 6063-T4 and 6063-W tubes, respectively. The bold numbers on the right half of each figure indicate the thickness measurements from FE simulations. Both the above numerical and experimental thickness measurements are plotted graphically in Fig. 9(d) as a function of position (see Fig. 9(c)). Clearly, there is good agreement in the results for both heat-treated conditions. Note that the thickness strain allowed in both situations was equal to a value of approximately  $-n/2$  as stated before. With the  $n$  values of AA6063 in the W-temper and T4 conditions as 0.34 and 0.26, respectively, the minimum thickness allowed in the T branch in the simulations is 2.26 mm and 2.60 mm, respectively. With these differences in allowed thinning, one can conclude that a higher T bulge can be formed with the W-temper material as shown in Fig. 9.

## 6 Discussion

It is evident from the results of the closed die hydroforming (Fig. 7) that there are distinct differences in the observed final hardness under each heat-treated condition. The tubes hydro-

**Table 4 Composition of AA6063 [19]**

Element	Al	Mg	Si	Cr, Mn Ti, Cu, Zn	Fe	Others
Wt. %	97.5	0.45–0.9	0.2–0.6	Max 0.1	Max 0.35	Max 0.15

formed in the T4 condition acquire a higher hardness than those hydroformed in the W temper. It is also evident that no amount of natural aging brings the hardness of the hydroformed tube in the W temper up to the level of the tubes formed in the T4 condition. Therefore, forming operation on materials in the W temper has a detrimental effect on the hardness and hence yield strength of the final component. Although these results could be expected, the current study quantifies this increase in hardness in the hydroformed components. There is an overall 17% increase in hardness when formed in the T4 condition compared to that in the W-temper condition. As the material ages, the microstructural kinetics play a dominant role in determining the forming characteristics and the hardness of the given alloy. To further understand the reasons for the observed behavior, a brief discussion on the related strengthening mechanisms and the relevant microstructural kinetics is given below.

The composition of AA6063 is given in Table 4 [19]. The main strengthening elements in any aluminium 6xxx series alloys are magnesium (Mg) and silicon (Si). Other elements, such as chromium (Cr), manganese (Mn), and titanium (Ti) are added to control grain structure, copper (Cu) to improve mechanical properties, and zinc (Zn) for corrosion resistance. Iron (Fe) is a common impurity in these metals [19]. The solution treatment and quenching operations result in a supersaturated solid solution in the material. All of the Mg and Si atoms are trapped in the solid solution and a supersaturated vacancy concentration is retained in the material. Upon aging, the solute Mg and Si atoms cluster at these vacancies to form Guinier Preston (GP) zones [20]. These zones are the locations for the precipitation of the intermediate  $\beta$  phases of  $Mg_2Si$  during the aging process. These submicron precipitates which form in the aluminum matrix are hard and hinder the dislocation motion through the aluminum matrix (during a forming operation). Therefore, additional stress is required for continued dislocation motion during plastic deformation. Thus, a fine dispersion of these precipitates, which results from the completion of the above aging process, produces a stronger material (T4). This behavior is evident from the tensile curves shown in Fig. 4, where the yield strength of the material increases with aging time, but the work hardening rate decreases. If the aging of the material is interrupted by cold work, for example via tensile deformation or hydroforming, the hardness of the final component is affected as shown in Fig. 7.

The serrated flow observed in the tensile stress–strain response (Fig. 4) has been well investigated in the literature. The phenomenon is called the PLC effect [21] which is a result of the interaction of the Mg and Si atoms with dislocation motion in the aluminium matrix during dynamic strain aging. During plastic deformation (in tensile testing) the solute atoms (i.e., Mg and Si atoms) attach to the dislocations and hinder their movement. As the tensile load is increased, the dislocations break free from these solutes. This process is reflected as a sudden load drop in the stress–strain response. As the tensile loading continues, this interaction repeats several times resulting in serrated flow.

As the material is aged for longer periods of time, the amount and the frequency of these serrations during tensile loading is reduced and the stress–strain curves exhibit a smoother response. This smooth response is due to the initiation of the precipitation process and the subsequent reduction in the number of free solute atoms that have not clustered into GP zones. Therefore, as the material is aged to the T4 condition, no PLC effect is noticed in the tensile response and the yield strength of the material is increased to more than twice the yield strength of the W-temper

alloy. Thus, the formed GP zones and/or intermediate precipitates dramatically increase the strength of the material.

The dynamic strain aging can be advantageous in some situations. Recall from Fig. 5 that material tested immediately upon quenching exhibits low yield strength and high work hardening coefficient ( $n$ ) close to 0.34. A higher  $n$  value is beneficial in forming processes as it increases the amount of uniform plastic strain which enlarges the process window and facilitates the formation of complex geometries. However, plastic work immediately after quenching can cause loss of strength in the material as observed in the hardness measurements on closed-die hydroforming (W\_HF\_AGE) (see Fig. 7). This result can be rationalized based on the hardening kinetics discussed above. After the quenching operation, the material has a fine dispersion of vacancies and has Mg and Si in solid solution. During forming operations in this condition (i.e., introduction of plastic work) dislocations moving through the aluminum lattice annihilate the vacancies that are essential for further hardening of the material. Without these vacancies, the sites for the formation of GP zones and precipitates do not exist and the material hardens only due to work hardening during the forming operation, i.e., increased dislocation density due to dislocation interaction and multiplication. It is shown in Fig. 7 that if the material is first aged to T4 condition prior to hydroforming, higher hardness values are obtained in the components. This result is due to the fact that the majority of the precipitation process has already occurred in the material, and therefore dislocations must cut through the GP zones or intermediate phase particles. This phenomenon results in higher material yield strength and hence higher loads are required for continued plastic flow of the material. Therefore, material formed in the T4 condition exhibits higher hardness (and yield strength) than seen in the W temper.

Finally, it should be noted that the material in the W-temper condition has a higher  $n$  value which allows for a larger process window and hence for the formation of a higher T branch as shown in Fig. 9. Thus, a tradeoff on strength for ductility should be made to form a complex part in the W temper.

## 7 Conclusions

Based on the above results and discussions, several conclusions can be drawn on material behavior and process optimization.

1. The tensile behavior of AA6063 was systematically analyzed in W temper through T4 conditions. Power-law model fit to the tensile stress–strain curves revealed that higher ductility (or higher hardening exponents) can be realized in the W-temper condition than in the T4 condition, thus increasing the process window to form complex geometries during hydroforming.
2. An optimization method was developed using LS-OPT and LS-DYNA to predict the process paths during hydroforming of a central bulge in a die cavity and to maximize a T branch in aluminum tubes.
3. In the optimization method, by choosing appropriate objectives and constraints, one can obtain strains that exceed the traditional forming limits. Therefore, more complex geometries can be formed using optimization methods. Well-coordinated process feed paths result in good conformance of the tube to the closed-die geometry and the development of a higher T branch.
4. Although a higher ductility can be realized in the W-temper

condition, components formed in the T4 condition exhibit higher hardness than those formed in the W-temper condition.

## Acknowledgment

The authors sincerely acknowledge the support from Hydro Aluminum Technology Center, N.A. and the Norwegian Research Council, Oslo, Norway.

## References

- [1] Liu, S.-D., Meuleman, D., and Thompson, K., 1998, "Analytical and Experimental Examination of Tubular Hydroforming Limits," *J. Mater. Manuf.*, **107**, pp. 287–297.
- [2] Rimkus, W., Bauer, H., and Mihsein, M. J. A., 2000, "Design of Load-Curves for Hydroforming Applications," *J. Mater. Process. Technol.*, **108**, pp. 97–105.
- [3] Yang, J.-B., Jeon, B.-H., and Oh, S.-I., 2001, "Design Sensitivity Analysis and Optimization of the Hydroforming Process," *J. Mater. Process. Technol.*, **113**, pp. 666–672.
- [4] Manabe, K.-i., and Amino, M., 2002, "Effects of Process and Material Properties on Deformation Process in Tube Hydroforming," *J. Mater. Process. Technol.*, **123**, pp. 285–291.
- [5] Fann, K.-J., and Hsiao, P.-Y., 2003, "Optimization of Loading Conditions for Tube Hydroforming," *J. Mater. Process. Technol.*, **140**, pp. 520–524.
- [6] Aue-U-Lan, Y., Ngaile, G., and Altan, T., 2004, "Optimizing Tube Hydroforming Using Process Simulation and Experimental Verification," *J. Mater. Process. Technol.*, **146**, pp. 137–143.
- [7] Imaninejad, M., Subhash, G., and Loukus, A., 2004, "Experimental and Numerical Investigation of Free-Bulge Formation During Hydroforming of Aluminum Extrusions," *J. Mater. Process. Technol.*, **147**, pp. 247–254.
- [8] Imaninejad, M., Subhash, G., and Loukus, A., 2004, "Influence of End-Conditions During Tube Hydroforming of Aluminum Extrusions," *Int. J. Mech. Sci.*, **46**, pp. 1195–1212.
- [9] Imaninejad, M., Subhash, G., and Loukus, A., 2005, "Load Path Optimization of Tube Hydroforming Process," *Int. J. Mach. Tools Manuf.*, **45**, pp. 1504–1514.
- [10] Asnafi, N., and Skogsgårdh, A., 2000, "Theoretical and Experimental Analysis of Stroke-Controlled Tube Hydroforming," *Mater. Sci. Eng., A*, **279**, pp. 95–110.
- [11] Koç, M., Aue-u-lan, Y., and Altan, T., 2001, "On the Characteristics of Tubular Materials for Hydroforming—Experimentation and Analysis," *Int. J. Mach. Tools Manuf.*, **41**, pp. 761–772.
- [12] Johnson, K. I., Nguyen, B. N., Davies, R. W., Grant, G. J., and Klialeel, M. A., 2004, "A Numerical Process Control Method for Circular Tube Hydroforming Prediction," *Int. J. Plast.*, **20**, pp. 1111–1137.
- [13] Chow, C. L., and Yang, X. J., 2002, "Bursting for Fixed Tubular and Restrainted Hydroforming," *J. Mater. Process. Technol.*, **130**, pp. 130–131.
- [14] Al-Qureshi, H. A., and Moriera Filho, L. A., 2001, "Junction Forming in Aluminum Tubes Using an Elastomer Technique," *Mater. Manuf. Processes*, **16**, pp. 717–724.
- [15] Loukus, A. R., Subhash, G., and Valberg, H., 2006, "The Influence of Pre-forming on Hydroforming of Extruded Aluminum Tubes," *Int. J. Form. Processes*, **9**(1), pp. 97–119.
- [16] Portevin, A., and LeChatelier, F., 1923, "Serrated Flow in Metals," *Comp. Rend. Acad. Sci.*, **176**, pp. 507.
- [17] Hatch, J. E., 1984, *Aluminum: Properties and Physical Metallurgy*, American Society for Metals, Metals Park, Ohio.
- [18] Marciniak, Z., and Duncan, J. L., 1992, *Mechanics of Sheet Metal Forming*, Edward Arnold, London.
- [19] Polmear, I. J., 1995, *Light Alloys, Metallurgy of the Light Alloys*, Butterworth Heinemann, Oxford.
- [20] Srivatsan, T. S., Sudarshan, T. S., Harvey, D. P., Jr., and Lavernia, E. J., 1993, "Strengthening Mechanisms and Deformation Characteristics of Wrought Aluminum Alloys," *Met., Mater. Processes*, **4**, pp. 259–286.
- [21] Reed-Hill, R. E., and Abbaschian, R., 1992, *Physical Metallurgical Principles*, 3rd ed., Van Nostrand, Princeton, NJ, pp. 294–298.